Quantitative imaging of boron, calcium, magnesium, potassium, and sodium distributions in cultured cells with ion microscopy. Anal Chem

ARTICLE *in* ANALYTICAL CHEMISTRY · JANUARY 1990

Impact Factor: 5.64 · DOI: 10.1021/ac00199a002 · Source: PubMed

4 AUTHORS, INCLUDING:

Subhash Chandra
Cornell University
78 PUBLICATIONS **1,687** CITATIONS

Quantitative Imaging of Boron, Calcium, Magnesium, Potassium, and Sodium Distributions in Cultured Cells with Ion Microscopy

Walter A. Ausserer,[1] Yong-Chien Ling,[2] Subhash Chandra, and George H. Morrison*

Baker Laboratory of Chemistry, Cornell University, Ithaca, New York 14853-1301

A method for the conversion of intensity information in ion micrographs of freeze-fractured, freeze-dried cultured cells to local dry weight elemental concentrations is presented. Homogenates generated from cultured cells are used as calibration standards. Ion microscope (IM) relative sensitivity factors for B, Ca, K, Mg, and Na with respect to the matrix element C are determined by the correlation of IM and inductively coupled plasma atomic emission spectrometry analyses of the cellular homogenates. After calibration of the IM imaging system, the relative sensitivity factors are used to determine local intracellular concentrations of B, Ca, K, Mg, and Na in cultured Swiss 3T3 fibroblasts. Intracellular B was introduced through cellular uptake of $Na_2B_{12}H_{11}SH$, a candidate therapeutic agent for boron neutron capture cancer therapy. The IM intracellular concentration results show good agreement with published electron probe X-ray microanalysis results. Estimated detection limits are in the low- to sub-parts-per-million dry weight concentration range.

INTRODUCTION

The ion microscope (IM) is a secondary ion mass spectrometer with elemental imaging capabilities (*1*, *2*). The distributions of many elements in biological samples are easily measured with the IM, which produces real-time images of elemental (isotopic) distributions at a spatial resolution of less than 1.0 μm. Analytical techniques that can perform highly sensitive elemental determinations in microscopic sample regions are needed for the study of elements in animal cells, because elemental concentrations are often tightly regulated in cellular subcompartments. Although the high elemental sensitivity and good spatial resolution of the IM make it a promising tool for such studies, several analytical problems have prevented quantitative elemental imaging of biological soft tissue samples with the IM from becoming routine. First, the sample preparation method must preserve native elemental distributions within the sample. Second, corrections for the influence of local matrix effect variations on local secondary ion signals must sometimes be made (*3-5*). Additionally, a quantification microstandard in which the matrix composition closely matches that of the sample must be available.

Several recent biological IM studies have employed thin sections of animal tissue (*6-11*). As an alternative to tissue work, a cryopreparation method for cultured animal cells has been developed in our laboratory (*12*). Cultured cells provide an excellent model system for the study of diverse physiological phenomena under well-controlled experimental conditions. Briefly, cells prepared by our method are cultured on high-purity silicon wafers and rapidly frozen to immobilize diffusible intracellular ions. The frozen samples are then sandwich-fractured under liquid nitrogen and freeze-dried at -100 °C prior to analysis. During the fracturing process, the apical cell surface and the adhering cell growth medium are removed, exposing the cellular interior for microanalysis, free from contamination. Previous IM studies of cells prepared by this method (fractured cells) found that local matrix effect variations are typically undetectable, so that matrix effect correction schemes are not required (*13*, *14*). The present study was undertaken to investigate the quantitative relationship between secondary ion signals and local concentrations of Na, Mg, K, Ca, and B in fractured cells.

There is widespread interest in the determination of intracellular levels of Na, Mg, K, and Ca because these are the major diffusible cations in biological systems. Our interest in the quantitative localization of intracellular B stems from recent progress in boron neutron capture therapy (BNCT), a promising strategy for the treatment of several types of human tumors (*15*). This therapy requires the selective incorporation of ^{10}B into tumor cells, with subsequent irradiation of the tumor with thermal neutrons. It is proposed that tumor cells can be selectively destroyed by the energetic products of the $^{10}B(n,\alpha)^7Li$ reaction. The intracellular distribution of B is important in BNCT because cell-killing efficiency is believed to depend on the proximity of the $^{10}B(n,\alpha)^7Li$ reaction to the genetic material of the cell.

In the present study, quantification microstandards are generated from homogenates of cultured cells. Relative sensitivity factors (RSF's) for the analytes with respect to the matrix element C are determined by correlation of IM and inductively coupled plasma atomic emission spectrometry (ICP-AES) analyses. Calibration of the IM imaging system for quantitative work is described, along with the application of imaging mode RSF's for the determination of local intracellular concentrations of B, Na, Mg, K, and Ca in cultured 3T3 fibroblasts. For B localization experiments, cells are incubated with $Na_2B_{12}H_{11}SH$, a candidate BNCT compound for the treatment of brain tumors.

EXPERIMENTAL SECTION

Sample Preparation. Quantification microstandards were prepared from cultured Swiss 3T3 mouse fibroblasts and from NRK-49F normal rat kidney fibroblasts. Swiss 3T3 cells were obtained from the laboratory of Efram Racker at Cornell University and NRK-49f cells from the American Type Culture Collection. Both cell lines were cultured in Dulbecco's modified Eagle's medium with 10% fetal bovine serum, 20 mM Hepes, 20 mM penicillin, and 100 μg/mL streptomycin (all from Gibco Laboratories). Cells were plated at a density of 1×10^5 cells/flask and cultured as monolayers in 150-cm^2 flasks. When confluency was approached, cells from eight flasks were detached by treatment with 0.25% trypsin in Ca- and Mg-free Dulbecco's phosphate buffered saline (Gibco), transferred to 50-mL polypropylene centrifuge tubes, collected by centrifugation at 900 rpm (Sorvall H1000B rotor) for 5 min, and drained. To remove the adhering trypsin solution, cells were twice resuspended in 30 mL of 160 mM $NH_4C_2H_3O_2$ and centrifuged as above. After thorough draining of the $NH_4C_2H_3O_2$ solution, the cell pellet was frozen

[1] Current address: Life Sciences Division, SRI International, 333 Ravenswood Ave., Menlo Park, CA 94025.
[2] Current address: Department of Chemistry, National Tsing Hua University, Hsinchu 30034, Taiwan, ROC.

0003-2700/89/0361-2690$01.50/0

and finely ground with a cold mortar and pestle in a liquid nitrogen trough. The ground cellular material was transferred to a cold 1.5-mL polypropylene tube, thawed, and spiked with B from a 1 mM $Na_2B_{12}H_{11}SH$ (Callery Chemical Co.) solution. To maximize elemental homogeneity, the cellular material was twice passed through a cycle of thawing, vigorous mixing with a micropipet, rapid freezing, and regrinding. The ground cells were then lyophilized. Being a volatile salt, the $NH_4C_2H_3O_2$ is removed from the sample during lyophilization, so that the remaining cellular homogenate was composed of relatively uncontaminated cellular material (*16, 17*). The lyophilized cell homogenate was mounted for IM analysis by firmly pressing small particles of the homogenate between the polished faces of two clean 1-cm^2 silicon pieces (General Diode Corp.) with a Parr Instrument Co. Model 2811 pellet press.

The bulk of the lyophilized homogenate was analyzed by ICP-AES. Samples, approximately 15 mg dry weight, were digested to near dryness in HF cleaned quartz tubes with 0.2 mL of concentrated HNO_3 (J. T. Baker Chemical Co.), which had been double distilled and condensed in Teflon. The digestate was cooled and diluted with 0.15 mL of 37% HCl (Baker) and 2.85 mL of H_2O. Digested samples were clear and contained no visible particulate matter. As verification of the digestion and ICP-AES procedures, NBS SRM 1571 (orchard leaves) and SRM 1573 (tomato leaves) were digested and analyzed exactly as the cell homogenates.

The preparation of fractured cell monolayers has been previously described (*12*). Swiss 3T3 cells were plated onto 1-cm^2 polished silicon pieces in 5-mL culture dishes at a density of 5 × 10^4 cells/dish. The culture medium is described above. To facilitate the sandwich fracture, 30 000 polystyrene beads (Duke Scientific Corp.) were added to each dish, with the bead diameter being 9.0 μm. The freezing medium was Freon-22 slush (Air Products and Chemicals, Inc.). For B localization experiments, 100 μg/mL $Na_2B_{12}H_{11}SH$ was added to the culture media 24 h after cell plating. Four days after plating, cells were frozen and freeze-fractured. Samples were freeze-dried at −100 °C for 24 h and analyzed directly on the silicon substrates.

ICP-AES Analysis. A Jarrell-Ash Model ICAP 61 Update was used for all ICP-AES measurements. A peristaltic pump operating at 2.5 mL/min introduced the samples into the spray chamber through a crossflow nebulizer. Calibration solutions were prepared in 5% HCl. Na, Mg, K, and Ca signals were calibrated from a multielement standard prepared from Na_2CO_3 and K_2CO_3 (Grade 1 Puratronic, Johnson Matthey Chemicals, Limited), 1000 ppm Mg and Mn atomic spectral standards (Baker), 99.999% Al powder, 99.999% $NH_4H_2PO_4$, 99.999% $(NH_4)_2SO_4$, 99.995% $CaCO_3$, and 99.999% Fe_2O_3 (all from Aldrich Chemical Co.). The B signal was calibrated with a multielement standard prepared from 99.999% H_3BO_3 (Aldrich), 99.999% Zn (Aldrich), and 1000 ppm Si, V, Cr, Co, Ni, Cu, As, Se, Y, Mo, Cd, and Pb atomic spectral standards (Baker). The analytical emission lines were 249.7 nm for B, 279.5 nm for Mg, 317.9 nm for Ca, 589.0 nm for Na, and 766.5 nm for K. All signals were blank and spectral interference corrected.

Ion Microanalysis. A Cameca IMS 3f secondary ion mass spectrometer with a mass filtered O_2^+ primary ion beam was used for secondary ion measurements. A primary beam diameter of 50 μm and a raster area of 250 × 250 μm were used for all experiments. Except where noted, the spectrometer was operated with 150-μm transfer optics, a 60-μm contrast aperture, a 1.8-mm field aperture, a 130-eV secondary ion energy window, and positive secondary ion detection with a pulse counting electron multiplier.

High-resolution mass scans ($m/\Delta m \approx 5000$) at nominal mass-to-charge ratios (m/z) of +10, +11, +12, +23, +24, +39, +40, and +41 were performed to check for mass interference components in the secondary ion signals from $^{10}B^+$, $^{11}B^+$, $^{12}C^+$, $^{23}Na^+$, $^{24}Mg^+$, $^{39}K^+$, $^{40}Ca^+$, and $^{41}K^+$. For these measurements, a 750-μm field aperture was used in the spectrometer. Samples of Swiss 3T3 homogenate (spiked to 1500 ppm B dry weight) and Swiss 3T3 fractured cells (incubated with 100 μg/mL $Na_2B_{12}H_{11}SH$) were analyzed at each m/z.

The energy distributions of secondary ions from Swiss 3T3 homogenate and Swiss 3T3 fractured cell samples were recorded to study the effect of the secondary ion energy window on relative ion signals. Two sets of spectra were recorded from each sample type, one with a primary ion beam of 100 nA and one with a 350-nA beam, resulting in four spectra for each m/z. The secondary ion energy window was set at ≈3 eV.

RSF Determination. RSF's for the analytes with respect to the matrix element carbon were determined by the analysis of three cell homogenate samples, two produced from Swiss 3T3 cells and one from NRK-49F's. Electron multiplier detection was used. Preliminary analyses of a Swiss 3T3 homogenate sample with primary beam currents of 100, 300, and 600 nA gave statistically identical RSF's for each analyte, so a 250-nA primary ion beam was used for all subsequent determinations. After samples were presputtered briefly to stabilize the secondary ion signals, signals at each m/z above were monitored cyclically for 1 s each for a total of 15 analysis cycles. RSF's for the relatively intense $^{23}Na^+$ and $^{39}K^+$ species were determined separately from the other analytes because of electron multiplier dynamic range considerations. In all cases, secondary ion signals were stable for the duration of the analysis. Values used for the calculation of RSF's were signals averaged over analysis cycles 6–15.

The RSF has generally been defined as

$$RSF_{x/ref} = (i_x/i_{ref})/(C_x f_x/C_{ref} f_{ref}) \quad (1)$$

where i is the secondary ion intensity, C is the elemental concentration, f is the isotopic abundance, x indicates the analyte, and ref indicates the reference species (*18, 19*). The slope of a plot of i_x/i_{ref} versus $C_x f_x/C_{ref} f_{ref}$ is therefore $RSF_{x/ref}$. The RSF's for the analytes with respect to the reference matrix element carbon reported here use a modified definition

$$RSF_{x/ref} = (i_x/i_{ref})/(f_x C_x) \quad (2)$$

so that $RSF_{x/ref}$ is not a true elemental RSF, but a calibration factor relating secondary ion i_x/i_{ref} ratios to C_x values determined by the ICP-AES analyses.

Ion Microscopy. Imaging experiments utilized the microchannel plate–phosphor screen detector (MCP–PS) of the Cameca IMS 3f. Images were acquired for digital image processing with a Photometrics, Ltd., Model CH220 CCD liquid-cooled camera head equipped with a Thomson-CSF TH7882CDA charge-coupled device (CCD). The CCD imager is not a video camera, but integrates images directly on the CCD chip. Image integration time is controlled by an electronic shutter. A Photometrics camera controller digitized the CCD output to 14 bits per pixel. Throughout this study, the CCD was operated in the 2 × 2 binning mode. The image processing system in our laboratory has been previously described (*20*). The ion pump for the 3f detector section was disabled during image acquisition to minimize stray ion background signal. The high sensitivity, wide dynamic range, and extremely linear response of scientific grade CCD imagers have been recently reviewed (*21–23*), and Mantus et al. (*24*) are preparing a paper that fully describes the performance of the CCD imager in ion microscopy. Single ion hits are easily detectable with this system because of its high sensitivity and very low noise level. The CCD imager exhibits near perfect response linearity over several orders of magnitude incoming light intensity and over integration times from 0.2 s to several minutes.

Imaging System Calibration. For application of the above-determined RSF's to the IM imaging system, calibration curves were constructed relating CCD pixel values to electron multiplier count rates for each m/z of interest. Curves were generated for two commonly used MCP gains, 60% (1748 V) and 70% (1956V). Gelatin films, doped with salts of the analyte elements, were deposited on 1-cm^2 silicon pieces and used as laterally homogeneous calibration standards. An IM magnification of 90× was used, so that the entire 1.35-cm-diameter ion image was centered on the 1.90-cm-diameter MCP-PS. Dark current corrected images were recorded at electron multiplier count rates of 1 × 10^3, 3 × 10^3, 1 × 10^4, and 3 × 10^4 counts/s for each m/z. In this signal range, the electron multiplier is essentially free from dead time. Calibration curves were constructed by plotting mean CCD pixel values per second (CCD_x) versus mean electron multiplier counts per pixel per second (EM_x). All curves were strongly linear and of the form

$$CCD_x = y_x EM_x + b_x \quad (3)$$

No dead time effects of the MCP-PS were detectable under these conditions.

Table I. Contribution of Analyte Ions to Secondary Ion Signals[a]

		% signal from analyte	
m/z	analyte	3T3 homogenate	3T3 fractured cells
10	$^{10}B^+$	>99.9	*b*
11	$^{11}B^+$	>99.9	*b*
12	$^{12}C^+$	99.8 (0.3)	>99.9
23	$^{23}Na^+$	>99.9	>99.9
24	$^{24}Mg^+$	96.9 (0.7)	98.5 (0.2)
39	$^{39}K^+$	>99.9	>99.9
40	$^{40}Ca^+$	96.9 (0.7)	97.0 (0.2)
41	$^{41}K^+$	98.6 (0.6)	99.8 (0.0)

[a] Values are reported as mean (standard deviation); n = 3. [b] Insufficient signal for high mass resolution spectrum.

Quantitative Imaging of Intracellular Elements. A primary ion beam of 250 nA was used for the acquisition of ion micrographs of control and $Na_2B_{12}H_{11}SH$-treated Swiss 3T3 fibroblasts. After brief sample presputtering, $^{11}B^+$, $^{12}C^+$, $^{23}Na^+$, $^{24}Mg^+$, $^{40}Ca^+$, and $^{41}K^+$ micrographs were recorded with the MCP gain fixed at 60%. Image acquisition times were 150.0 s for $^{11}B^+$, 60.0 s for $^{12}C^+$, 0.4 s for $^{23}Na^+$, 30.0 s for $^{24}Mg^+$, 30.0 s for $^{40}Ca^+$, and 3.0 s for $^{41}K^+$. $^{41}K^+$ was monitored rather than the more intense $^{39}K^+$ to avoid saturation of the CCD imager. The generation of concentration information from these images required three operations: (1) spatial registration of the analyte image and the $^{12}C^+$ reference image to permit ratioing of signals from exactly corresponding areas, (2) calculation of the mean CCD pixel values per second for identical sample features of interest in the analyte image (CCD_x) and the $^{12}C^+$ reference image (CCD_{ref}), and (3) conversion of the signal ratio CCD_x/CCD_{ref} to analyte dry weight concentration as shown below.

Rearranging eq 2 and inserting EM_x and EM_{ref} for i_x and i_{ref} produce

$$C_x = (EM_x/EM_{ref})/(f_x RSF_{x/ref}) \quad (4)$$

Combining eq 3 and 4, one obtains

$$C_x = (CCD_x - b_x)y_{ref}/[(CCD_{ref} - b_{ref})y_x f_x RSF_{x/ref}] \quad (5)$$

In practice, b_x and b_{ref} are negligibly small as compared to CCD_x and CCD_{ref}, so eq 5 simplifies to

$$C_x = CCD_x y_{ref}/[CCD_{ref} y_x f_x RSF_{x/ref}] \quad (6)$$

RESULTS AND DISCUSSION

Ion Microanalysis. Table I lists the results of high-resolution mass scans for Swiss 3T3 homogenate and Swiss 3T3 fractured cell samples. Each value is the mean result of three scans. Mass scans from the homogenate and fractured cell samples are generally in close agreement, with the secondary ion signals being composed of >96% analyte ions in all cases. Although corrections for mass interference contributions to secondary ion signals can be incorporated in quantification algorithms, no corrections have been employed in this study because the contributions are relatively small.

Secondary ion energy distributions from Swiss 3T3 homogenate and Swiss 3T3 fractured cell samples are shown in Figure 1. Energy spectra from the two sample types were indistinguishable, as were spectra produced with the different primary ion beam intensities. Each curve in Figure 1 is a smoothed point-by-point average of the four spectra recorded at each m/z, where the raw spectra were scaled to 2×10^6 total counts prior to averaging. The low-energy tails were all very weak and have been omitted. The resultant curves for $^{23}Na^+$ and $^{39}K^+$ were superimposable, as were the curves for $^{24}Mg^+$ and $^{40}Ca^+$. The prominence of the high-energy spectral tail correlates with the chemical group of the element, being least prominent for the alkali metals and most prominent for $^{12}C^+$.

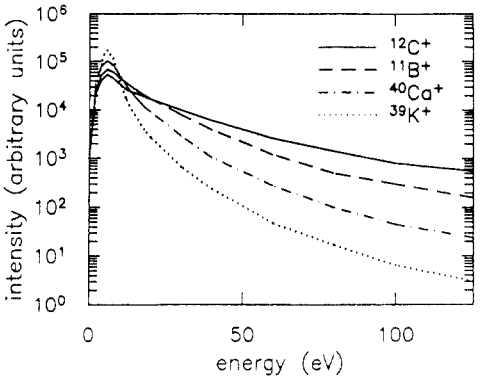

Figure 1. Secondary ion energy distributions. Each curve is a smoothed average of four spectra as described in the text, scaled to 2×10^6 total counts for ease of comparison.

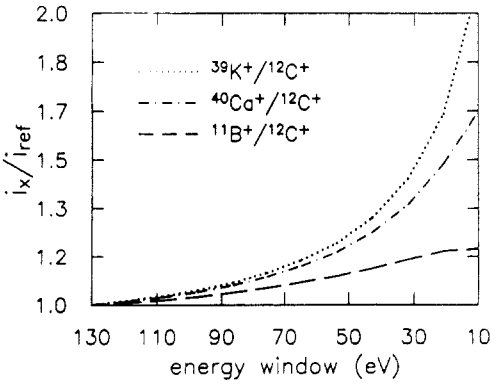

Figure 2. Variation of analyte-to-carbon ratios as the spectrometer energy window is narrowed from 130 to 10 eV. Curves were generated from the normalized data presented in Figure 1, so that a ratio of 1.0 is imposed at an energy window setting of 130 eV for each curve.

The IM secondary ion energy window is variable from 0 to 130 eV, with image resolution generally improving as the window is narrowed. Because the different analyte ions exhibit different energy distributions, decreasing the energy band-pass will attenuate the different analytical signals nonuniformly. The variation of signal ratios of $^{39}K^+$, $^{40}Ca^+$, and $^{11}B^+$ to $^{12}C^+$ as a function of energy window setting is shown in Figure 2. These curves were generated from the data plotted in Figure 1, except that the spectra were scaled to the same total counts in a 130-eV energy window centered on the spectral peak. Note that analyte-to-carbon signal ratios can increase dramatically as the energy window is narrowed. In this study, we have determined RSF's for the analytes ratioed to the matrix element C with the energy window set at 130 eV. Figure 2 demonstrates that these RSF values will be valid only when a 130-eV band-pass is used.

RSF Determination. To validate the digestion and ICP-AES procedures, NBS SRM 1571 (orchard leaves) and SRM 1573 (tomato leaves) were digested and analyzed exactly as the cell homogenates. The results are listed in Table II. Of particular interest were the B values, because loss of B during wet ashing is a well-known problem. The results in Table II indicate that significant loss of B did not occur during digestion.

Table III lists IM analyte-to-carbon ratio results (i_x/i_{ref}), ICP-AES concentration results (C_x), and calculated $RSF_{x/ref}$ values from analysis of the cell homogenate samples. As anticipated, the IM sensitivity decreases dramatically with increasing first ionization potential of the analyte. Because of imperfect elemental homogeneity, relatively large standard deviations are associated with the IM results, particularly with the higher concentration Na and K values. The $RSF_{x/ref}$ values calculated from the three samples are identical for each analyte

Table II. Analysis of NBS SRM's for Validation of ICP-AES Procedures[a]

analyte	certified composition (dry wt)	ICP-AES results (dry wt)
	NBS SRM 1571: Orchard Leaves	
B	33 (3) μg/g	31.9 (0.1) μg/g
Na	82 (6) μg/g	67 (1.3) μg/g
Mg	0.62 (0.02)%	0.678 (0.003)%
K	1.47 (0.03)%	1.64 (0.01)%
Ca	2.09 (0.03)%	2.23 (0.01)%
	NBS SRM 1573: Tomato Leaves	
K	4.46 (0.03)%	4.54 (0.02)%
Ca	3.00 (0.03)%	3.20 (0.01)%
Mg	0.7%[b]	0.731 (0.003)%
B	30 μg/g[b]	32.6 (0.2) μg/g

[a] NBS values are reported as mean (uncertainty) as defined in the NBS Standard Reference Material Catalog. ICP-AES values are reported as mean (standard deviation) for four analyses. [b] Noncertified values.

within statistical uncertainty.

In applying the $RSF_{x/ref}$ values for the quantification of intracellular elemental concentrations, we have assumed that the $RSF_{x/ref}$ values are not dependent on analyte concentration. To test this assumption, the three homogenate samples were spiked with B levels of 359, 682, and 1329 ppm. Statistically identical $RSF_{x/ref}$ values were calculated for each, indicating a constant B $RSF_{x/ref}$ over this concentration range. Further studies to determine linear $RSF_{x/ref}$ ranges and cell-line-to-cell-line $RSF_{x/ref}$ variability are planned in our laboratory.

Imaging System Calibration. Table IV lists typical fitting parameters for the calibration of CCD pixel values to EM count rates at MCP gains of 1748 and 1958 V (gains of 60% and 70%, respectively). All curves are strongly linear, with the slopes at 70% gain being slightly more than twice the slopes at 60% gain. Lighter ions generally generate steeper calibration curves than heavier ones. The intercept values are very small compared to the maximum allowable CCD pixel value of 16 383, a result of the low noise character of the MCP–PS–CCD image detector combination. Because of their small magnitudes, the intercept values were found to have no statistically significant impact on the image quantification results presented below; i.e. the intercept term in the CCD pixel value to EM count rate linear calibration equation can be justifiably omitted.

Three calibrations were performed over a 6-week period to monitor calibration reproducibility. Individual calibration slopes varied significantly over this period, probably because the responses of the EM and MCP-PS slowly degrade with use. For the image quantification scheme investigated here, however, variation of the analyte calibration slopes with respect to the calibration slope of $^{12}C^+$ is the relevent calibration characteristic. Ratios of analyte slopes to carbon slope from the three calibration sessions are listed in Table V. No statistical difference was found between the two MCP gains. Reproducibility of analyte-to-carbon slope ratios is quite good, with relative standard deviations ranging from 1.1% to 8.5%. In practical terms, this indicates that frequent system calibration is not critical. This is fortuitous, because completion of the calibration procedure requires several hours of data acquisition and analysis.

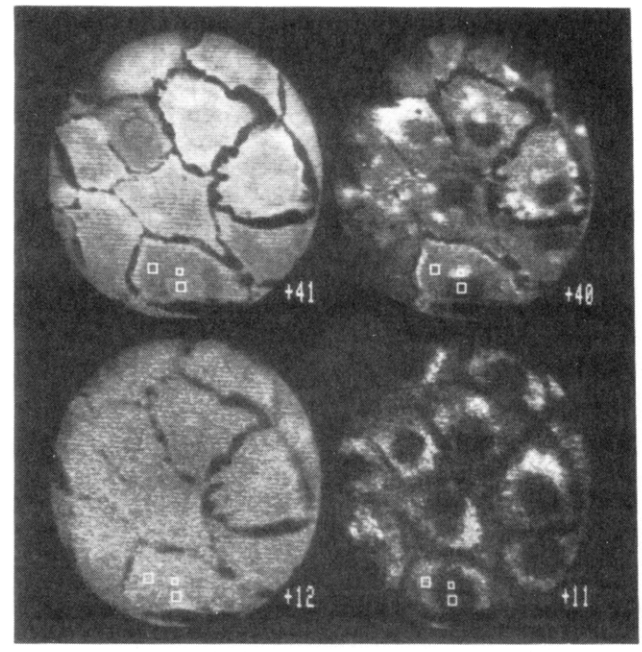

Figure 3. $^{41}K^+$, $^{40}Ca^+$, $^{12}C^+$, and $^{11}B^+$ ion micrographs from several Swiss 3T3 fibroblasts treated with 100 μg/mL $Na_2B_{12}H_{11}SH$. The three boxed areas in the lowest cell of each micrograph are included to illustrate analytical areas. In each micrograph, the lower right box denotes a cytoplasmic area, the upper right box a perinuclear area, and the upper left box a cytoplasmic area.

Quantitative Imaging of Intracellular Elements. Ion micrographs of $^{41}K^+$, $^{40}Ca^+$, $^{12}C^+$, and $^{11}B^+$ from several Swiss 3T3 fibroblasts treated with 100 μg/mL $Na_2B_{12}H_{11}SH$ are shown in Figure 3. Cell nuclei are easily discernible in the $^{40}Ca^+$ micrographs because nuclear Ca signals are low relative to cytoplasmic levels. A region adjacent to one side of the nucleus (perinuclear) exhibited markedly elevated $^{40}Ca^+$ signals in nearly all of the Swiss 3T3 fibroblasts analyzed.

Table III. Cell Homogenate Analyses: ICP-AES and IM Results with Calculated $RSF_{x/ref}$ Values[a]

		NRK1			NRK2			3T3		
analyte	f_x	i_x/i_{ref}	C_x, ppm	$RSF_{x/ref}$	i_x/i_{ref}	C_x, ppm	$RSF_{x/ref}$	i_x/i_{ref}	C_x, ppm	$RSF_{x/ref}$
$^{10}B^+$	0.20	2.4 (0.2) × 10^{-2}	359 (2)	3.4 (0.3) × 10^2	9.5 (0.9) × 10^{-2}	1329 (9)	3.6 (0.4) × 10^2	4.9 (0.5) × 10^{-2}	682 (4)	3.6 (0.4) × 10^2
$^{11}B^+$	0.80	9.0 (0.8) × 10^{-2}	359 (2)	3.1 (0.3) × 10^2	3.6 (0.3) × 10^{-1}	1329 (9)	3.4 (0.3) × 10^2	1.8 (0.2) × 10^{-1}	682 (4)	3.4 (0.4) × 10^2
$^{23}Na^+$	1.000	1.5 (0.4) × 10^2	3790 (40)	4.1 (1.1) × 10^4	1.7 (0.4) × 10^2	4220 (30)	4.1 (0.9) × 10^4	9.8 (2.3) × 10^1	2200 (20)	4.4 (1.1) × 10^4
$^{24}Mg^+$	0.7899	3.5 (0.3)	1134 (6)	3.9 (0.3) × 10^3	3.7 (0.4)	1143 (5)	4.1 (0.5) × 10^3	1.8 (0.2)	586 (3)	3.8 (0.4) × 10^3
$^{39}K^+$	0.9326	9.6 (2.4) × 10^1	2010 (90)	5.1 (1.3) × 10^4	8.9 (1.5) × 10^1	1830 (60)	5.2 (0.9) × 10^4		bdl[b]	
$^{40}Ca^+$	0.9694	7.4 (0.7) × 10^{-1}	83.6 (0.9)	9.1 (0.9) × 10^3	1.0 (0.1)	133.8 (0.1)	8.9 (1.0) × 10^3	8.8 (1.0) × 10^{-1}	98.0 (0.5)	9.3 (1.1) × 10^3
$^{41}K^+$	0.0673	6.1 (0.9)	2010 (90)	4.8 (0.7) × 10^4	6.7 (1.3)	1830 (60)	5.3 (1.0) × 10^4		bdl[b]	

[a] Values are reported as mean (standard deviation); $n = 9$ for i_x/i_{ref} entries; $n = 4$ for C_x entries. [b] bdl: signal below the ICP-AES detection limit.

Table IV. Linear Least-Squares Fitting Parameters for Typical Calibration Plots of CCD Pixel Values per Second versus EM Counts per Pixel per Second

	G_{MCP} = 1748 V			G_{MCP} = 1956 V		
analyte	slope	intercept	r	slope	intercept	r
$^{11}B^+$	69.41	−0.8919	0.99996	146.6	−2.543	0.99946
$^{12}C^+$	65.42	−0.9896	0.99996	134.6	−.5563	0.99999
$^{23}Na^+$	49.31	−0.2677	0.99995	110.8	−1.594	0.99978
$^{24}Mg^+$	51.27	−0.0628	0.99995	113.8	.0694	0.99997
$^{40}Ca^+$	42.33	0.4099	0.99993	97.30	−0.9351	0.99982
$^{41}K^+$	43.24	−0.5682	0.99998	94.16	0.3785	0.99999

Table V. Ratios of Analyte-to-Carbon Slopes from Three Calibrations of CCD Pixel Values to EM Count Rates Performed over a Six-Week Period[a]

	slope M^+/slope $^{12}C^+$	
analyte	G_{MCP} = 1748 V	G_{MCP} = 1956 V
$^{11}B^+$	1.07 (0.02)	1.08 (0.05)
$^{23}Na^+$	0.83 (0.06)	0.82 (0.01)
$^{24}Mg^+$	0.85 (0.06)	0.84 (0.01)
$^{40}Ca^+$	0.71 (0.06)	0.73 (0.02)
$^{41}K^+$	0.71 (0.05)	0.71 (0.02)

[a] Values are reported as mean (standard deviation).

Concentration data were therefore generated from three regions of each cell: nuclear, perinuclear, and cytoplasmic. These regions were identified by eye during image processing of the $^{40}Ca^+$ micrographs and delineated with boxes. After image registration, identical areas within the $^{11}B^+$, $^{12}C^+$, $^{23}Na^+$, $^{24}Mg^+$, and $^{41}K^+$ micrographs were also delineated. Boxes indicating the analytical areas are shown on a single cell in each ion micrograph in Figure 3 to illustrate this process. Dry weight analyte concentrations from similar regions in each analyzed cell were generated from eq 6. These calculations used y_x/y_{ref} values from Table V and $RSF_{x/ref}$ values of 3.3 × 10^2 for B, 4.2 × 10^4 for Na, 3.93 × 10^3 for Mg, 5.1 × 10^4 for K, and 9.1 × 10^3 for Ca.

The concentration results are listed in Table VI. Levels of K were roughly an order of magnitude higher than those of Na, in agreement with basic electrophysiology. While K, Na, and Mg exhibited reasonably homogeneous distributions, both Ca and B were distributed quite heterogeneously. It is particularly interesting to note that although both Ca and B were concentrated mainly in the cytoplasm, B levels were relatively low in the Ca-rich perinuclear region. Further studies of the uptake of boronated BNCT agents by tumor cells are in progress in our laboratory.

Because electron probe X-ray microanalysis (EPXMA) is currently the favored technique for cellular elemental microanalysis, a comparison of the IM data with published EPXMA values is warranted. A number of EPXMA studies of cultured cells have been published (e.g. ref 25–29), but most have used nonphysiological washing solutions such as $NH_4C_2H_3O_2$, NH_4NO_3, sucrose, or deionized water to remove the cellular nutrient medium. A recent study by Tvedt et al. avoided the use of washing solutions by using a perpendicular cryosectioning approach (*30*). Table VII presents comparison the EPXMA results of Tvedt et al. with our IM results. As is accepted practice in the EPXMA literature, values are reported as mmol/kg dry weight (standard error of the mean). There is good agreement between the two techniques, except that the IM Na levels are somewhat higher.

Although the IM is clearly an imaging technique with high elemental sensitivity, the estimation of detection limits for elements in the cellular matrix is problematic. Detection limits are typically defined as the concentration of an analyte that produces a signal equal to 2 or 3 times the standard deviation of the blank signal. Blanks for major physiological metals in the cellular matrix are not easily prepared. However, animal cells generally contain very little B, and so can be considered a suitable blank for the estimation of B detection limits. The standard deviation of pixel values from 20 × 20 pixel areas in three control Swiss 3T3 fibroblasts analyzed exactly as the other fibroblasts in this study averaged 15.3 pixel units (on a pixel unit scale of 0 to 16383). Raw $^{11}B^+$ signals averaging 757 pixel units were used to generate the 563 ppm cytoplasmic B level reported for $Na_2B_{12}H_{11}SH$ treated cells in Table VI. The B concentration that would give rise to a signal of 45.9 pixel units (3 times the standard deviation of the blank signal) is therefore 34 ppm dry weight. By use of the relative elemental sensitivities listed in Table III, detector calibration slopes from Table V, a 15.3 pixel unit blank standard deviation value, and an image acquisition time of 150 s, dry weight detection limit estimates of 0.36 ppm K, 0.40 ppm Na, 2.1 ppm Ca, and 4.0 ppm Mg can be calculated for the instrumental conditions used in this study. These values ignore spectral interferences and are presented only as very rough estimates. For comparison, an optimal detection limit of 1 mmol/kg dry weight is often quoted for biological EPXMA (*31*, *32*).

Several sources of uncertainty in our elemental quantification protocol should be pointed out. Our method assumes that the intracellular ^{12}C concentration is proportional to the cellular dry weight concentration at each resolvable location within the cell. Considering the moderate spatial resolving power of the IM, this is a good approximation. A second assumption is that the analyte signals are not dependent on the analyte's chemical state in the cellular matrix. This point is difficult to investigate, but the largely homogeneous IM images of K^+, Na^+, Mg^+, and C^+ obtained from fractured cells suggest an absence of significant chemical-state effects. Additionally, we have reported previously that small cytoplasmic granules may possess sputter rates differing from that of the general cytosol (*14*), so that the quantitative uncertainty associated with signals from small cytoplasmic structures is difficult to estimate. Because such structures are generally too small to be resolved by the IM, the effects of this phe-

Table VI. Dry Weight Elemental Concentration Results from Nuclear, Perinuclear, and Cytoplasmic Cellular Regions of Swiss 3T3 Fibroblasts[a]

	K, %	Na, %	Mg, %	Ca, ppm	B, ppm
		Control, n = 38			
nuclear	4.65 (0.9)	0.55 (0.18)	0.17 (0.02)	255 (43)	bdl[b]
perinuclear	4.09 (0.9)	0.59 (0.16)	0.15 (0.02)	455 (71)	bdl
cytoplasmic	4.44 (1.0)	0.65 (0.19)	0.18 (0.03)	355 (58)	bdl
		B Treated, n = 31			
nuclear	5.17 (1.3)	0.43 (0.12)	0.19 (0.03)	220 (46)	170 (40)
perinuclear	4.68 (1.1)	0.50 (0.17)	0.17 (0.03)	499 (110)	254 (60)
cytoplasmic	4.92 (1.1)	0.49 (0.12)	0.18 (0.03)	375 (89)	563 (160)

[a] Values are reported as mean (standard deviation). [b] bdl: below detection limit.

Table VII. Comparison of IM Elemental Concentration Results with X-ray Microanalysis Results of Tvedt et al.[a]

	K	Na	Mg	Ca	B
			Control, n = 38		
nuclear	1190 (38)	240 (12)	70 (1)	6.4 (0.2)	bdl
perinuclear	1150 (36)	260 (11)	62 (1)	11.4 (0.3)	bdl
cytoplasmic	1130 (43)	280 (14)	72 (2)	8.9 (0.2)	bdl
			B Treated, n = 31		
nuclear	1320 (59)	190 (9)	76 (2)	5.5 (0.2)	16 (1)
perinuclear	1200 (53)	220 (14)	69 (2)	12.4 (0.5)	23 (1)
cytoplasmic	1260 (49)	210 (10)	75 (2)	9.4 (0.4)	52 (3)
			Tvedt et al.[b]		
	1294 (37)	147 (31)	62 (3)	−1.0 (1.0)[c]	*d*

[a] Values are reported as mean mmol/kg dry weight (standard error of the mean). [b] n = 43; whole cell concentrations were reported. [c] Not significantly different from zero. [d] Not reported.

nomenon typically are not detectable.

The precision of our intracellular concentration results and their excellent agreement with values from the EPXMA literature argue that the above shortcomings are not serious, and that the IM is a reliable technique for cellular microanalysis. Strengths of the IM technique include a simple and quick sample preparation method for cultured cells, broad elemental scope, high elemental sensitivity, and the intuitive advantages of data which is output directly as real time images. The IM opens new avenues of biomedical research, because it can quantitatively image the distributions of many elements present in concentrations far below EPXMA detection limits. The capability of the IM to perform isotopic analyses additionally suggests exciting possibilities for the investigation of elemental homeostasis and transport with stable isotopes.

ACKNOWLEDGMENT

We gratefully acknowledge Ellie Kable and the Cornell Biophysics Tissue Culture Facility for culture assistance, David L. Miller and William Bauer of Idaho National Engineering Laboratory for preliminary ICP-AES studies, Mike Rutzke of the Pomology Analytical Laboratory at Cornell for the ICP-AES analyses used in this study, and David Mantus for many helpful discussions. We additionally thank K. E. Tvedt of the University of Trondheim and *Journal of Microscopy* for permission to include the EPXMA results.

LITERATURE CITED

(1) Rouberol, J. M.; Lepareur, M.; Autier, B.; Bourgot, J. M. *8th International Conference on X-Ray Optics and Microanalysis and 12th Annual Conference of the Microbeam Analysis Society*, Boston, MA, 1977; pp 133A–133D.
(2) Morrison, G. H.; Slodzian, G. *Anal. Chem.* **1975**, *47*, 932A–943A.
(3) Patkin, A. J.; Chandra, S.; Morrison, G. H. *Anal. Chem.* **1982**, *54*, 2507–2510.
(4) Burns, M. S.; File, D. M.; Deline, V.; Galle, P. *Scanning Electron Microsc.* **1986**, *IV*, 1277–1290.
(5) Brenna, J. T.; Morrison, G. H. *Anal. Chem.* **1986**, *58*, 1675–1680.
(6) Hallegot, P.; Galle, P. *Radiat. Environ. Biophys.* **1988**, *27*(1), 67–78.
(7) Schaumann, L.; Galle, P.; Thellier, M.; Wissocq, J. C. *J. Histochem. Cytochem.* **1988**, *36*(1), 37–39.
(8) Mentre, P.; Escaig, F. *J. Histochem. Cytochem.* **1988**, *36*(1), 49–54.
(9) Burns, M. S. *Soc. Neurosci. Abstr.* **1988**, *14*(1), 618.
(10) Fragu, P.; Larras-Regard, E. *Bio. Cell* **1988**, *62*(2), 145–155.
(11) Sod, E. W.; Morrison, G. H.; Crooker, A. R., submitted for publication in *J. Microsc. (Oxford)*.
(12) Chandra, S.; Morrison, G. H.; Wollcott, C. C. *J. Microsc. (Oxford)* **1986**, *144*, 15–37.
(13) Chandra, S.; Ausserer, W. A.; Morrison, G. H. *J. Microsc. (Oxford)* **1987**, *148*, 223–239.
(14) Ausserer, W. A.; Chandra, S.; Morrison, G. H. *J. Microsc. (Oxford)* **1989**, *154*, 39–57.
(15) *Neutron Capture Therapy*; Hatanaka, H., Ed.; MTP: Norwell, MA, 1986.
(16) Zierold, K.; Pietruschka, F.; Schafer, D. *Microsc. Acta* **1979**, *81*(5), 361–366.
(17) Ceder, O.; Roomans, G. M.; Hosli, P. *Scanning Electron Microsc.* **1982**, *II*, 723–730.
(18) Werner, H. W. *SIA, Surf. Interface Anal.* **1980**, *2*(2), 56–74.
(19) Ramseyer, G. O.; Morrison, G. H. *Anal. Chem.* **1983**, *55*, 1963–1970.
(20) Ling, Y.-C.; Bernius, M. T.; Morrison, G. H. *J. Chem. Inf. Comput. Sci.* **1987**, *27*, 86–94.
(21) Hiraoka, Y.; Sedat, J. W.; Agard, D. A. *Science* **1987**, *238*, 36–41.
(22) Sweedler, J. V.; Bilhorn, R. B.; Epperson, P. M.; Sims, G. R.; Denton, M. B. *Anal. Chem.* **1988**, *60*, 282A–291A.
(23) Aikens, R. S.; Agard, D. A.; Sedat, J. W. In *Methods in Cell Biology, Vol. 29, Fluorescence Microscopy of Living Cells in Culture, Part B*. Wang, Y. L., Taylor, D. L., Eds.; Academic: New York, 1989; pp 291–313.
(24) Mantus, D. S.; Turner, L. K.; Morrison, G. H., paper in preparation.
(25) James-Kracke, M. R.; Sloane, B. F.; Shuman, H.; Karb, R.; Somlyo, A. P. *J. Cell Physiol.* **1980**, *103*, 313–322.
(26) Wroblewski, J.; Roomans, G. M.; Madsen, K.; Friberg, U. *Scanning Electron Microsc.* **1983**, *II*, 777–784.
(27) Wroblewski, J.; Roomans, G. M. *Scanning Electron Microsc.* **1984**, *IV*, 1875–1882.
(28) Abraham, E. H.; Donovan, C. B.; Lange, D. E. In *Microbeam Analysis* **1984**; Romig, A. D., Goldstein, J. I. Eds.; San Francisco Press: San Francisco, CA, 1984; pp 285–289.
(29) Abraham, E. H.; Breslow, J. L. Epstein, J.; Chang-Sing, P.; Lechene, C. *Am. J. Physiol. (Cell Physiol.)* **1985**, *17*, C154–C164.
(30) Tvedt, K. E.; Halgunset, J.; Kopstad, G.; Haugen, O. A. *J. Microsc. (Oxford)* **1988**, *151*(1), 49–59.
(31) Hall, T. A. *Ultramicroscopy* **1988**, *24*, 181–184.
(32) Johnson, D.; Izutsu, K.; Cantino, M.; Wong, J. *Ultramicroscopy* **1988**, *24*, 221–236.

RECEIVED for review July 21, 1989. Accepted October 2, 1989. This work was supported by grants from the National Institutes of Health, the DOE-funded PBF/BNCT Program for Cancer Treatment, and the National Science Foundation. The Cornell NIH/NSF Developmental Resource for Biophysical Imaging and Optoelectronics was used in culturing the cells.